

H9 GRANT

IN-34-CR

128069
18P

**FINITE ELEMENT METHODS OF ANALYSIS FOR
HIGH SPEED VISCOUS FLOWS**

Final Report for the Period 1 October 1986: 30 September 1987

Prepared for the

**Aerothermal Loads Branch
Loads and Aeroelasticity Division
NASA Langley Research Center
Hampton, Virginia 23665, U.S.A.**

GRANT NAGW-478 Supplement 3

**Submitted by the
Institute for Numerical Methods in Engineering
University of Wales
Swansea SA2 8PP
United Kingdom**

**(NASA-CR-182529) FINITE ELEMENT METHODS OF
ANALYSIS FOR HIGH SPEED VISCOUS FLOWS Final
Report, 1 Oct. 1986 - 30 Sep. 1987 (Wales
Univ.) 18 p**

CSCI 20D

N88-18852

G3/34 0128069

Unclass

INTRODUCTION

Over the past three years we have been developing a finite element based procedure for the solution of high speed viscous compressible flows. The approach followed has been to compute steady state solutions via a false transient, using an explicit time stepping scheme, and to attempt to improve the solution quality by incorporating adaptive mesh procedures. This strategy has been shown to be very successful in the context of the compressible Euler equations and also for some simple compressible viscous flows. The main thrust of our work over the past twelve months has been to work on the extension of the approach to the solution of some realistic compressible viscous flows. When flows at high Reynolds number are investigated, it soon becomes apparent that explicit techniques have to be supplemented if they are to deal effectively with the large variations in element size and aspect ratio which characterise the computational grids necessary for adequate resolution of the primary flow features. For this reason, our basic Taylor-Galerkin solution algorithm has been re-written in an explicit/implicit form. A structured grid is laid down in the vicinity of solid walls and the remainder of the flow field is covered by an unstructured assembly of triangles. In the unstructured grid region the basic explicit solver is employed, while the implicit version is used in the structured portion of the grid. The solution of the implicit equation system is achieved by directional splitting, using a block tridiagonal solver. Using this approach, solutions have been computed for the problems of (i) flow past a flat plate, M-3, Re-1000 (ii) shock/ boundary layer interaction, M-2, Re-296000 (iii) flow over a compression corner, M-11.68, Re-246000 (iv) uniform flow past a circular cylinder, M-6.34, Re-39770. A summary of the results produced is included in this report and demonstrates the numerical performance of the scheme.

IMPLICIT/EXPLICIT SOLUTION SCHEME

A description of the scheme will be given for the Euler equations. The extension [1,2] to the Navier-Stokes equations follows directly, but the algebra becomes rather messy. The form of the scheme was suggested by the original work of Lerat et al [3,4]. The governing equations are assumed in the form

$$\frac{\partial \underline{U}}{\partial t} + \frac{\partial F_j}{\partial x_j} = 0$$

where, in the usual notation, \underline{U} denotes the vector of conserved variables and F_j denotes the flux component in direction x_j of a Cartesian coordinate system. Using a Taylor series expansion about time $t - t_n$ gives

$$\underline{U}^{n+1} = \underline{U}^n + \Delta t \left. \frac{\partial \underline{U}}{\partial t} \right|^n + \frac{\Delta t^2}{2} \left[(1-\theta) \left. \frac{\partial^2 \underline{U}}{\partial t^2} \right|^n + \theta \left. \frac{\partial^2 \underline{U}}{\partial t^2} \right|^{n+1} \right]$$

and, using the governing equation, we can write

$$\frac{\partial U}{\partial t} = - \frac{\partial F_j}{\partial x_j} \quad \frac{\partial^2 U}{\partial t^2} = \frac{\partial}{\partial x_i} \left[A_i \frac{\partial F_j}{\partial x_j} \right]$$

The time stepping scheme then becomes

$$\begin{aligned} \Delta U - \theta \frac{\Delta t^2}{2} \frac{\partial}{\partial x_i} \left[A_i^n A_j^n \frac{\partial}{\partial x_j} (\Delta U) \right] \\ = - \Delta t \frac{\partial F_j^n}{\partial x_j} + \frac{\Delta t^2}{2} \frac{\partial}{\partial x_j} \left[A_j^n \frac{\partial F_i^n}{\partial x_i} \right] \end{aligned}$$

The solution of this equation system is achieved in a two-stage manner:

STAGE 1... explicit predictor

$$\Delta U_{exp} = - \Delta t \frac{\partial F_j^n}{\partial x_j} + \frac{\Delta t^2}{2} \frac{\partial}{\partial x_j} \left[A_j^n \frac{\partial F_i^n}{\partial x_i} \right]$$

This stage is performed using the two step Taylor-Galerkin code that has formed the basis of our previous work.

STAGE 2...implicit corrector

The implicit corrector is only employed on the structured grid and the equation system is solved by directional splitting in the form

$$\Delta U^* - \theta \frac{\Delta t^2}{2} \frac{\partial}{\partial x_1} \left[(A_1^n)^2 \frac{\partial}{\partial x_1} (\Delta U^*) \right] = \Delta U_{exp}$$

$$\Delta U - \frac{\theta \Delta t^2}{2} \frac{\partial}{\partial x_2} \left[(A_2^n)^2 \frac{\partial}{\partial x_2} (\Delta U) \right] = \Delta U^*$$

To reduce the computational cost, these equations are formed using the finite difference approach. Note however that at steady-state the solution satisfies

$$\Delta U_{exp} = 0$$

APPLICATIONS

The results produced by applying the above algorithm to a series of viscous flow problems will now be shown.

(i) flow over a flat plate, M-3, Re-1000. A regular mesh of 56*50 points and 5600 elements was employed (see Figure 1). Points were clustered near the leading edge and near the plate. Isothermal wall conditions were applied on the plate with symmetry conditions ahead of the nose of the plate. The use of a regular mesh means that the implicit scheme can be applied everywhere or only locally. Figures 2 and 3 show the density and pressure contours when 15 layers near the plate are treated implicitly with a Courant number C-5. A comparison between the behaviour of the fully implicit, mixed implicit/explicit and fully explicit schemes is made in Figures 4-7 in terms of the convergence behavior, exit density and x_1 velocity profiles and plate pressure distribution. Figures 8-10 show the comparison between the results of Carter [5] and the computations performed at ALB, LaRC for the same quantities. It may be observed that the rates of convergence of the fully implicit and the mixed explicit/implicit schemes are approximately equal, while the fully explicit algorithm shows a much slower convergence behaviour with peculiar oscillatory behaviour (which may be caused by an inappropriate artificial viscosity model for highly stretched grids).

(ii) shock/boundary layer interaction, M-2, Re-296000. The computation corresponds to the experiments of Hakkinen et al [6] and the Reynolds number is based upon the distance of the shock impingement point from the leading edge of the plate. The shock is of sufficient strength to cause separation of the developing laminar boundary layer. The first mesh employed consists of a regular grid of 32*45 points, equally spaced in the x_1 direction and exponentially stretched in the x_2 direction. The grid is shown in Figure 11 and the computed pressure and Mach number contours produced by the fully implicit procedure are shown in Figures 12 and 13. Adaptive remeshing was now performed, producing the mesh of 3293 points shown in Figure 14. On this grid the solution was advanced at C-5 in the 21 layers nearest the plate and the final pressure and Mach number contours are given in Figures 15 and 16. The computed variation in the static pressure and the skin friction along the plate are shown in Figures 17 and 18 respectively. The results obtained on the second mesh have been found to agree well with the computed results of MacCormack [7] and Dawes [8]. Details of the velocity profiles in the vicinity of the separation point can be seen in Figure 19.

(iii) flow over a compression corner, M-11.68, Re-246000. The intention was to compute the configuration tested by Holden [9] but it has been recently discovered that the computed compression corner angle was 14.5 degrees which differed from the 15 degrees in the actual experiment. Consequently, this problem is currently being recomputed for the

correct geometry and with an improved mesh. We present the results for the incorrect geometry as an example of the computational performance. An initial solution was produced on a regular mesh, equally spaced in the x_1 direction and exponentially stretched in the x_2 direction. The computed solution on this mesh was used to start the adaptive refinement process. The final mesh employed is shown in Figure 20 and the solution was advanced with C-5 in the 24 structured layers along the wall. Density and pressure contours are shown in Figures 21 and 22 and the distributions of pressure and skin friction along the wall are given in Figures 23 and 24. The computed region of separated flow is smaller than that observed experimentally which suggests insufficient mesh resolution in the vicinity of the corner.

(iv) undisturbed flow past a cylinder, M-6.34, Re-39770. The problem was initially solved inviscidly and the mesh adapted for the bow shock. A structured mesh was then constructed in the vicinity of the cylinder and consisted of 15 layers of elements. The final mesh employed had 4312 points. The solution was advanced with C-5 in the structured grid region and explicitly over the remainder of the grid. The final mesh and the computed contours of density and Mach number are shown in Figures 25-27. The computed distributions of pressure and heating rate over the cylinder surface are displayed in Figures 28 and 29 and are in good agreement with the results produced for this problem at ALB, LaRC.

CONCLUSIONS

A mixed explicit/implicit algorithm for the solution of problems involving high speed compressible viscous flows has been presented. Initial tests with the method have proved to be encouraging and the approach is being tested and extended further. In particular, the need for employing a structured grid and the finite difference discretisation in the implicit region is being reviewed with the objective of producing an implicit method for unstructured grids.

REFERENCES

- [1] O. Hassan, Ph.D. Thesis, University of Wales, Swansea (in preparation).
- [2] O. Hassan, K.Morgan and J.Peraire, ' An implicit/explicit scheme for compressible viscous flows', to be submitted to Int.J.Num.Meth. Engng., 1988.
- [3] A.Lerat, J.Sides and V.Daru, ' Efficient computation of steady and unsteady transonic flows by an implicit solver', in Advances in Computational Transonics (edited by W.G.Habashi), Pineridge Press, 543-575, 1985.
- [4] H.Hollanders, A.Lerat and R.Peyret, ' 3D calculation of transonic viscous flows by an implicit method', AIAA Paper 83-1953, 1983.
- [5] J.B.Carter, 'Numerical solutions of the Navier-Stokes equations for the supersonic laminar flow over a two-dimensional compression corner', NASA TR R-385, 1972.
- [6] R.J.Hakkinen, I.Greber, L.Trilling and S.S.Abarbanel, 'The interaction of an oblique shock wave with a laminar boundary layer', NASA Memo 2-18-59W, 1959.

- [7] R.W.MacCormack, 'A numerical method for solving the equations of compressible viscous flow', AIAA J. 20, 1275-1281, 1982.
- [8] W.N.Dawes, 'Efficient implicit algorithm for the equations of 2D viscous compressible flow: application to shock-boundary layer interaction', Int.J.Heat and Fluid Flow 4, 17-25, 1983.
- [9] M.J.Holden, 'A study of flow separation in regions of shock wave-boundary layer interaction in hypersonic flow', AIAA Paper.

ADDITIONAL PUBLICATIONS

- [1] R.Lohner, K.Morgan, J.Peraire and M.Vahdati, 'Finite element flux corrected transport for the Euler and Navier-Stokes equations', Int.J.Num.Meth.Fluids, 7, 1093-1109, 1987.
- [2] J.Peraire, K.Morgan and O.C.Zienkiewicz, 'Convection dominated problems', in Numerical Methods for Compressible Flows - Finite Difference, Element and Volume Techniques, ASME AMD-Vol 78, 129-147, 1986.
- [3] O.C.Zienkiewicz, K.Morgan, J.Peraire and J.Zhu, 'Some expanding horizons for computational mechanics - error estimates, mesh generation and hyperbolic problems', in Computational Mechanics - Advances and Trends, ASME AMD-Vol 75, 281-297, 1986.
- [4] K.Morgan, J.Peraire, J.Peiro and O.C.Zienkiewicz, 'Adaptive remeshing applied to the solution of a shock interaction problem on a cylindrical leading edge', to appear in the Proceedings of the Joint IMA/SMAI Conference on Computational Methods in Aeronautical Fluid Dynamics, Oxford University Press, 1988.
- [5] J.Peraire, K.Morgan, J.Peiro and O.C.Zienkiewicz, 'An adaptive finite element method for high speed flows', AIAA Paper 87-0559, 1987.
- [6] J.Peiro, L.Formaggia, J.Peraire and K.Morgan, 'Finite element solutions of the Euler equations in 2 and 3D', 7th GAMM Conference on Numerical Methods in Fluid Mechanics, 1987.
- [7] K.Morgan, J.Peraire, R.R.Thareja and J.R.Stewart, 'An adaptive finite element scheme for the Euler and Navier-Stokes equations', AIAA Paper 87-1172-CP, 1987.
- [8] K.Morgan and J.Peraire, 'Finite element methods for compressible flows', von Karman Institute for Fluid Dynamics Lecture Series 1987-04, 1987.

ORIGINAL PAGE IS
OF POOR QUALITY.

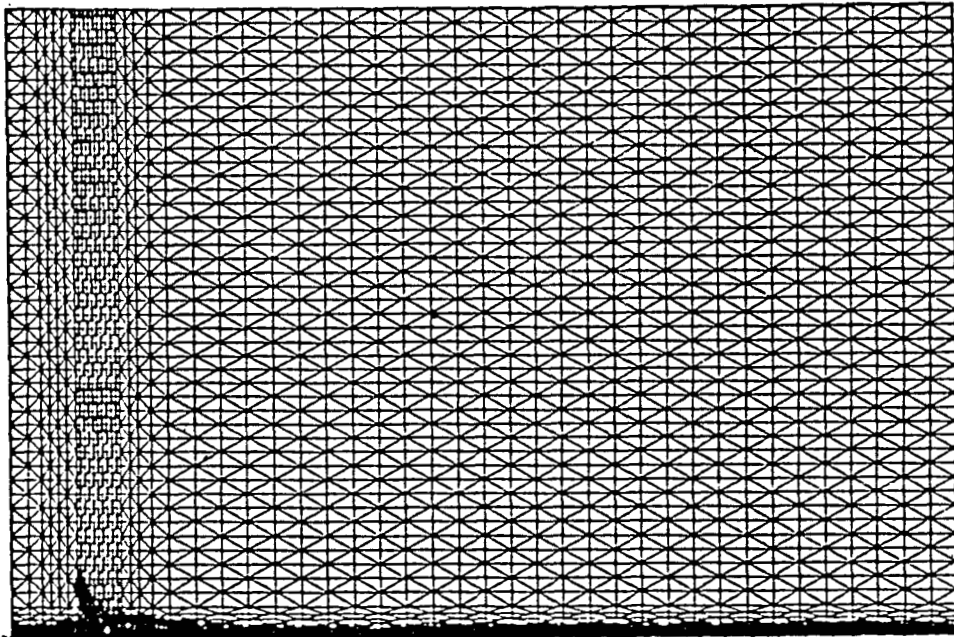
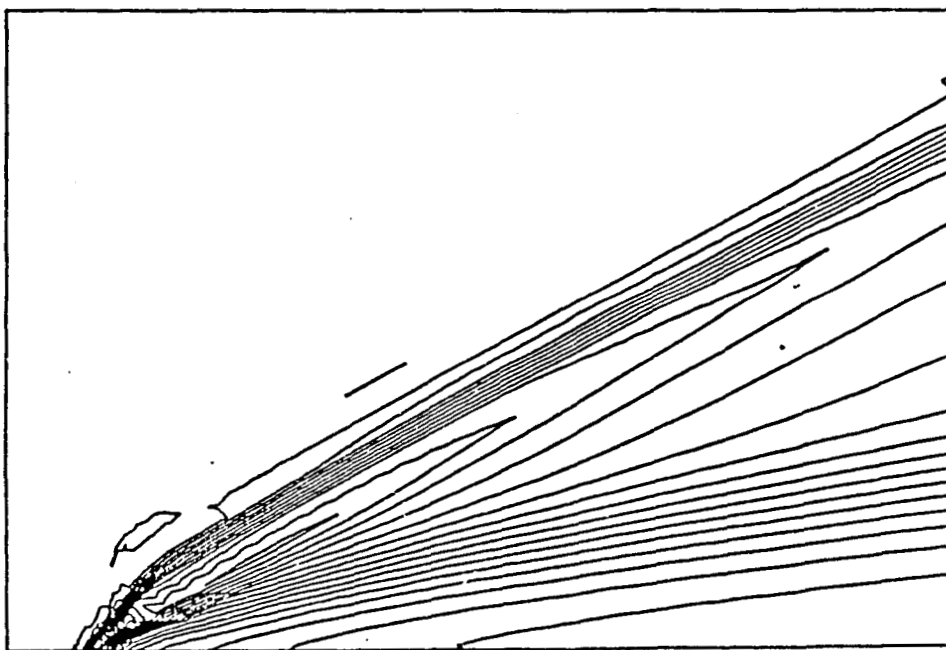
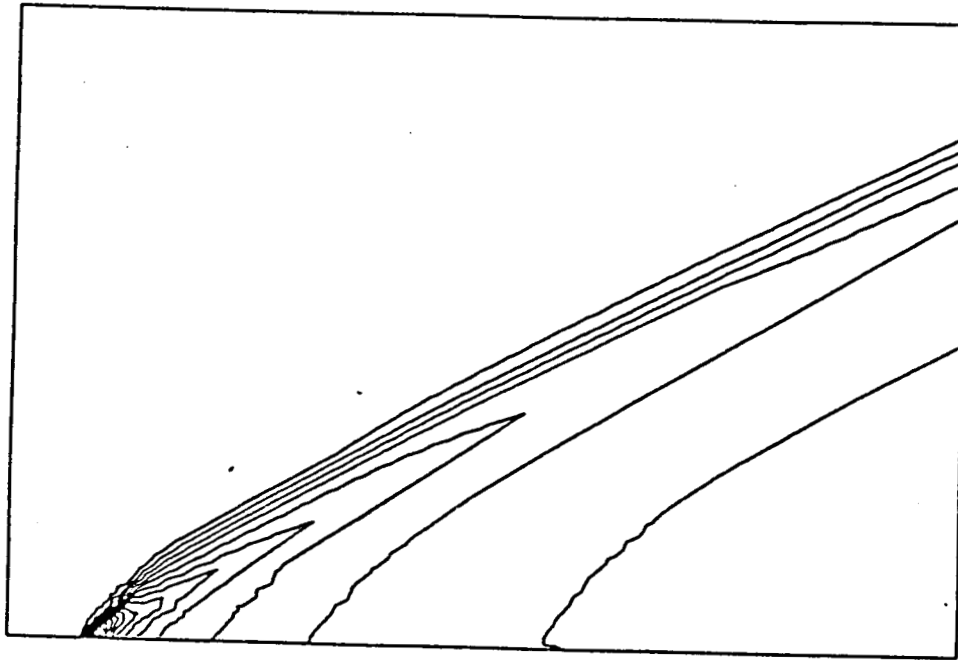


FIGURE 1



DENSITY

FIGURE 2



PRESSURE

FIGURE 3

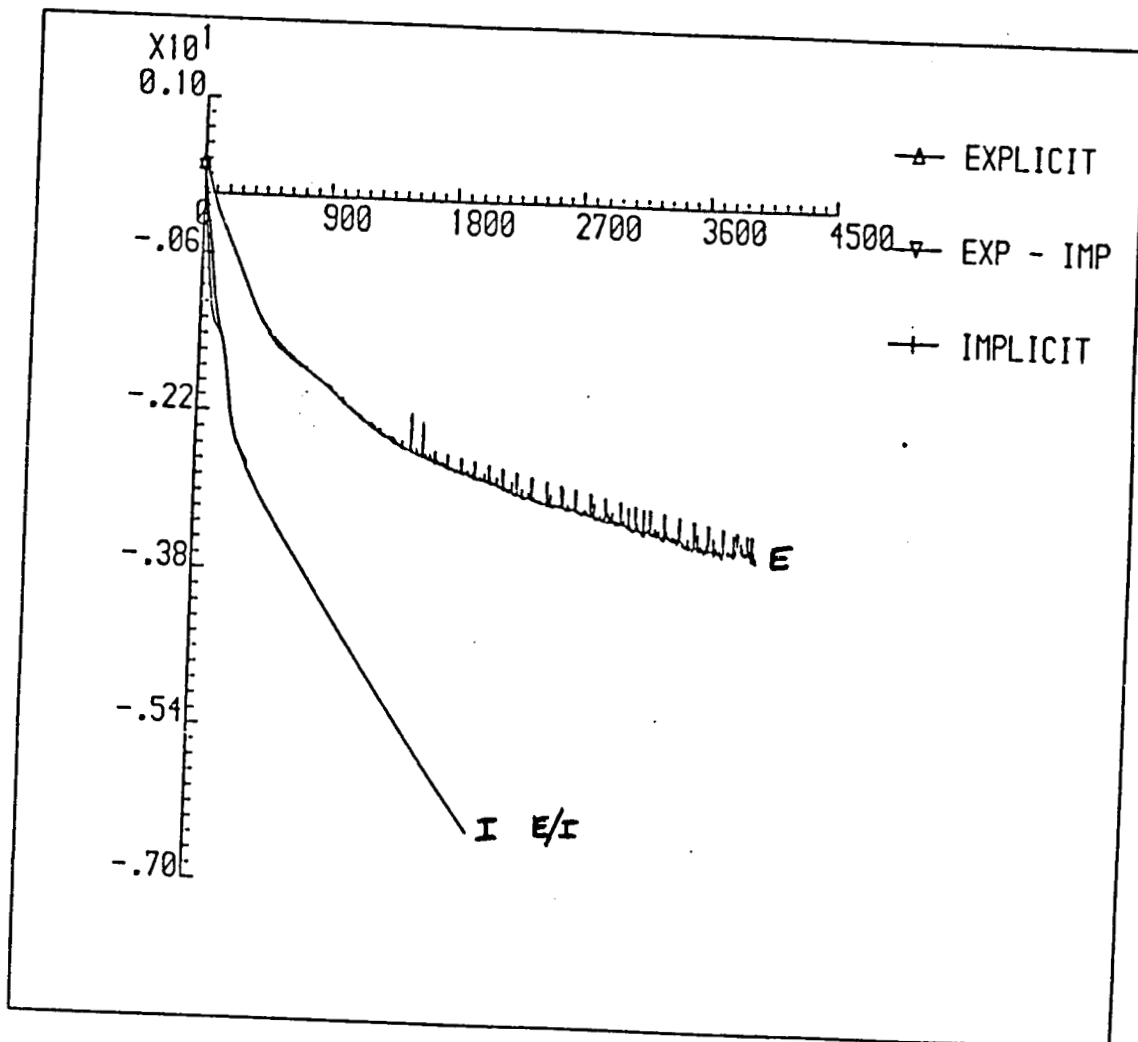


FIGURE 4

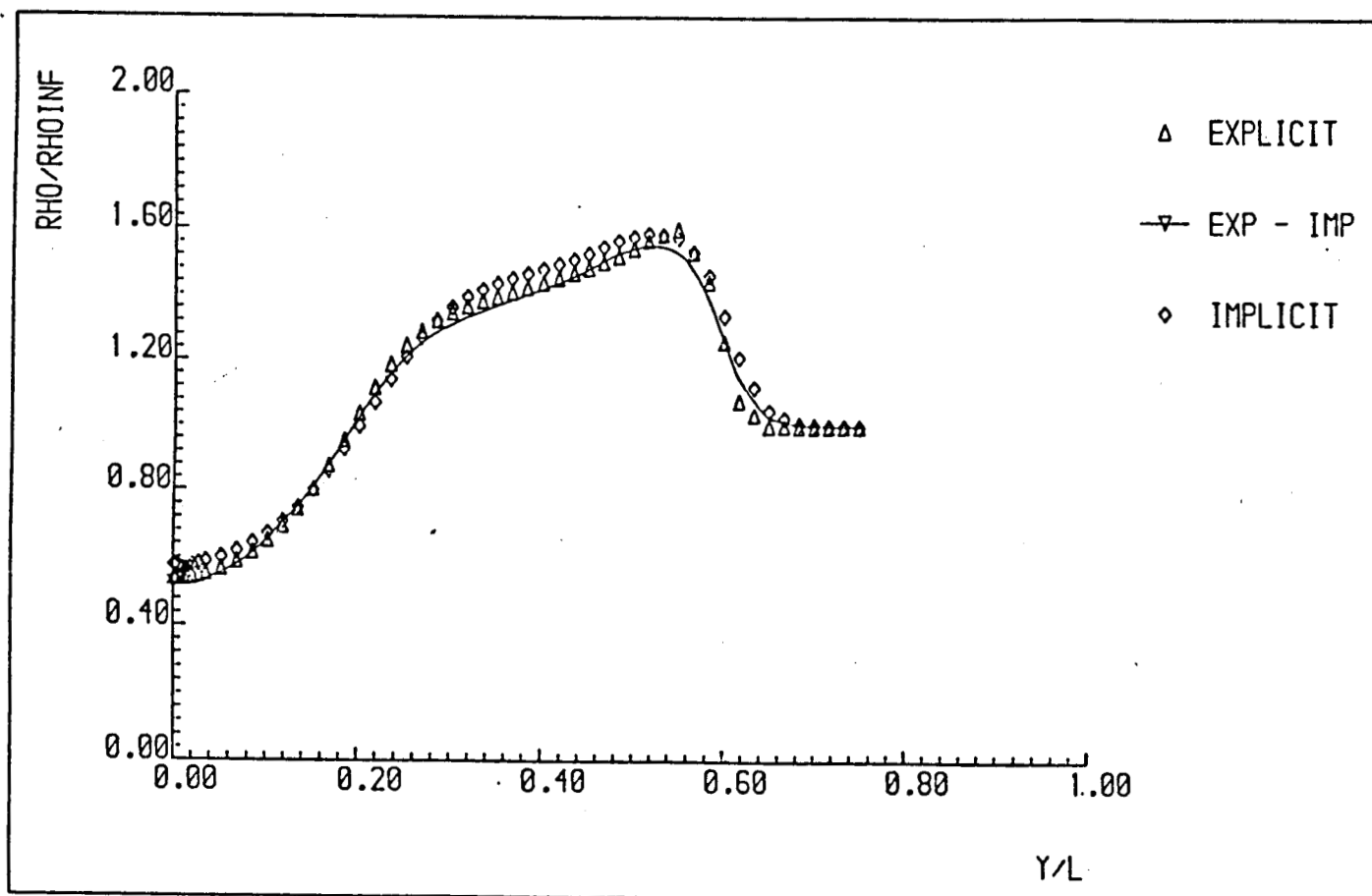


FIGURE 5 EXIT DENSITY PROFILE

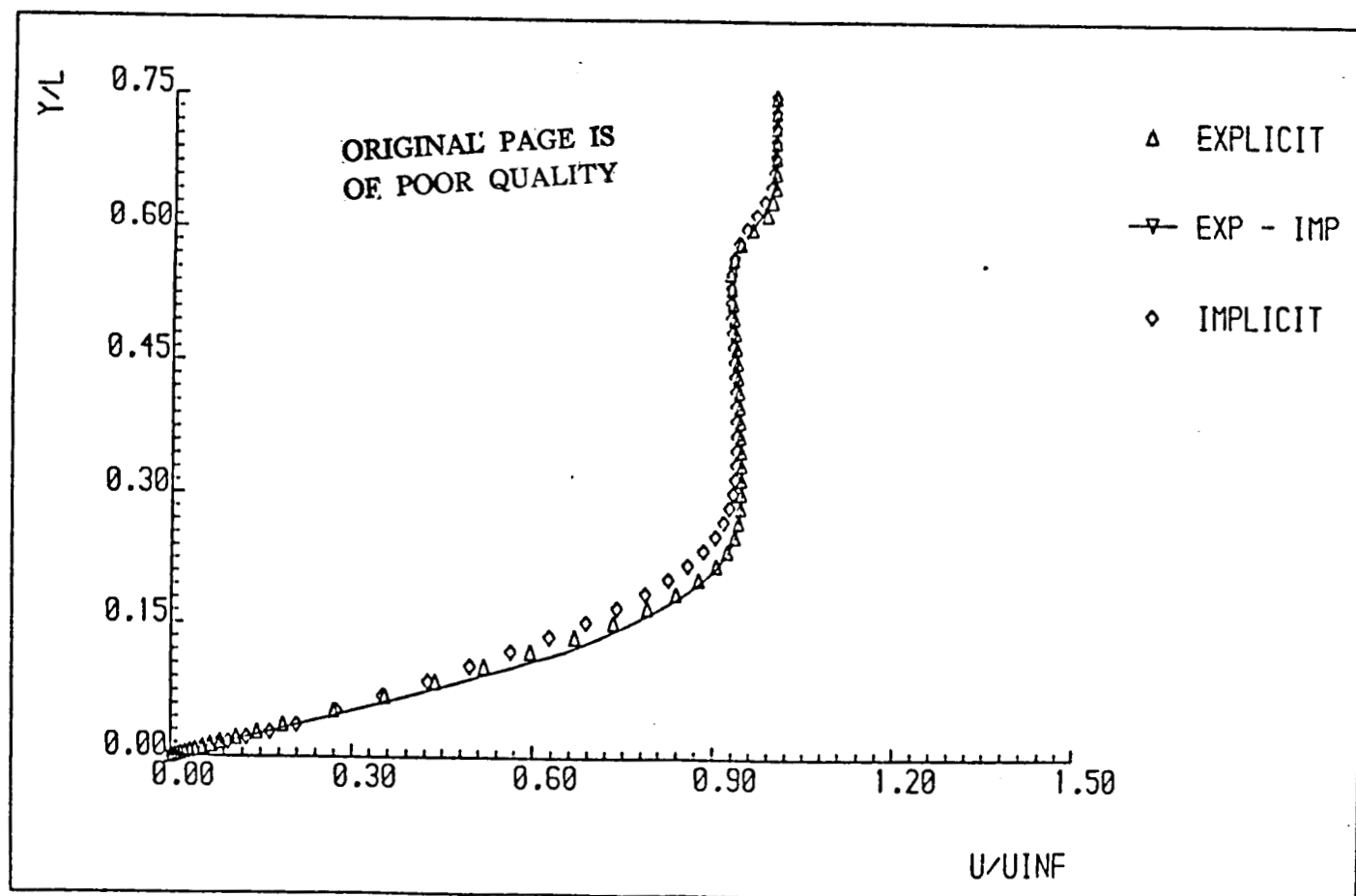


FIGURE 6 EXIT U-VELOCITY PROFILES

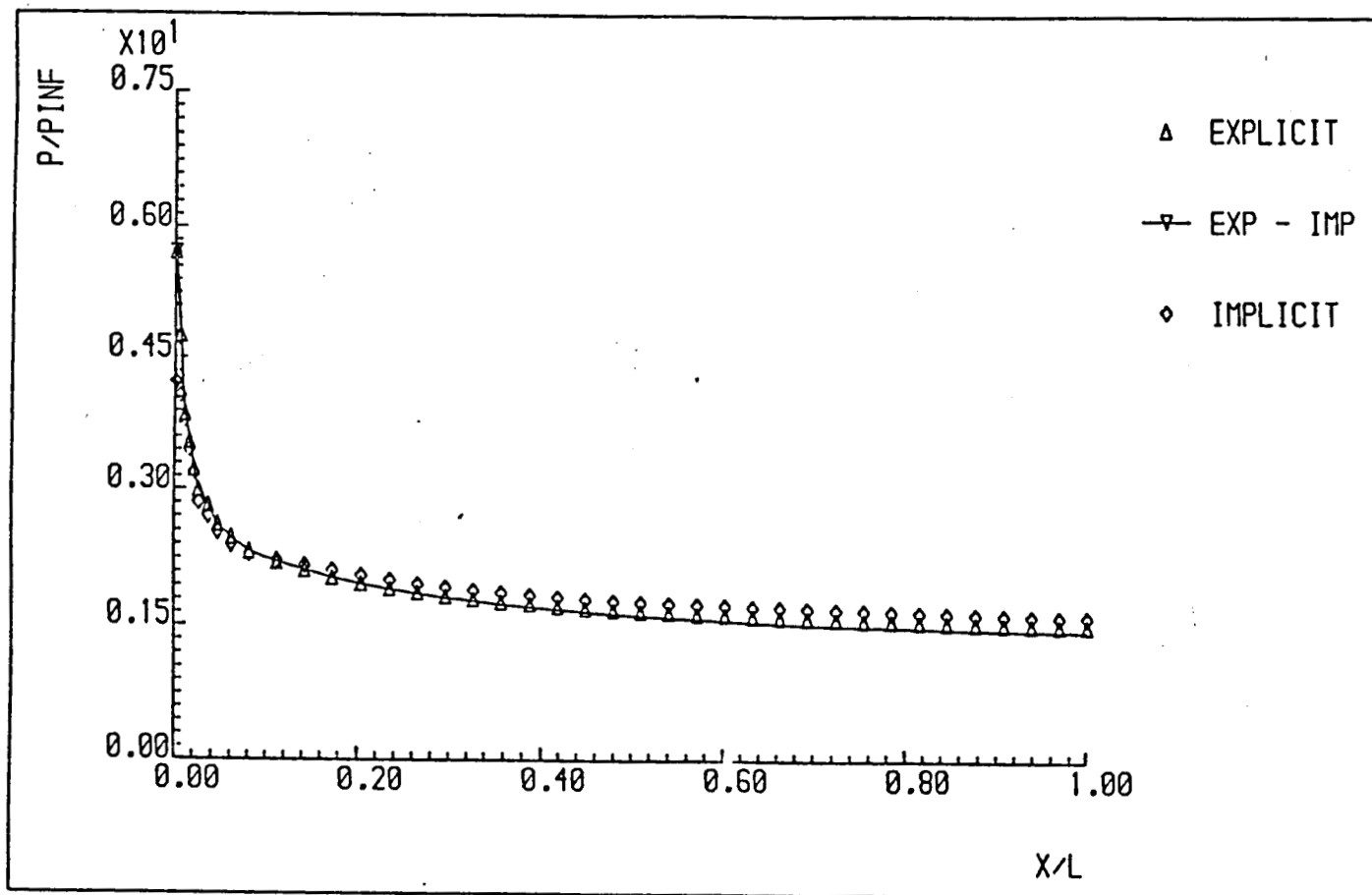


FIGURE 7 WALL PRESSURE DISTRIBUTIONS

EXIT DENSITY PROFILE

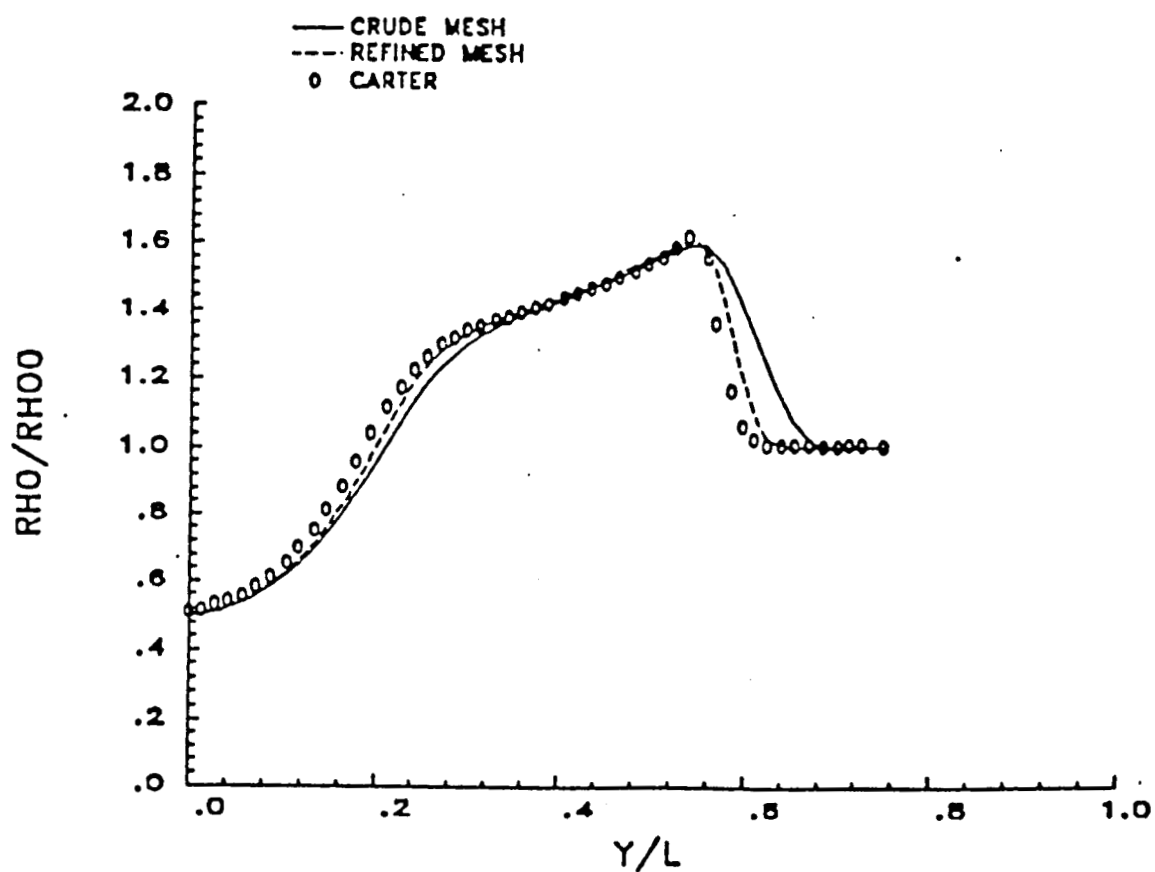


FIGURE 8

EXIT U-VELOCITY PROFILES

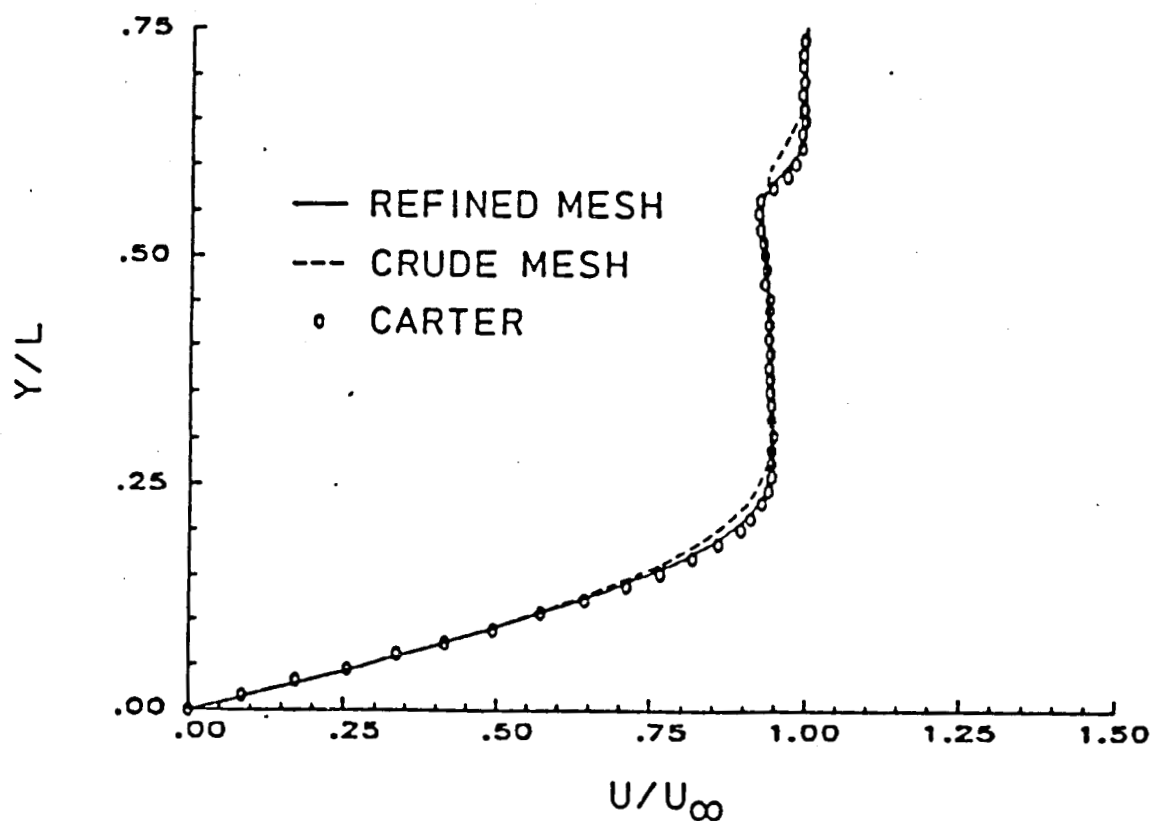


FIGURE 9

WALL PRESSURE DISTRIBUTIONS

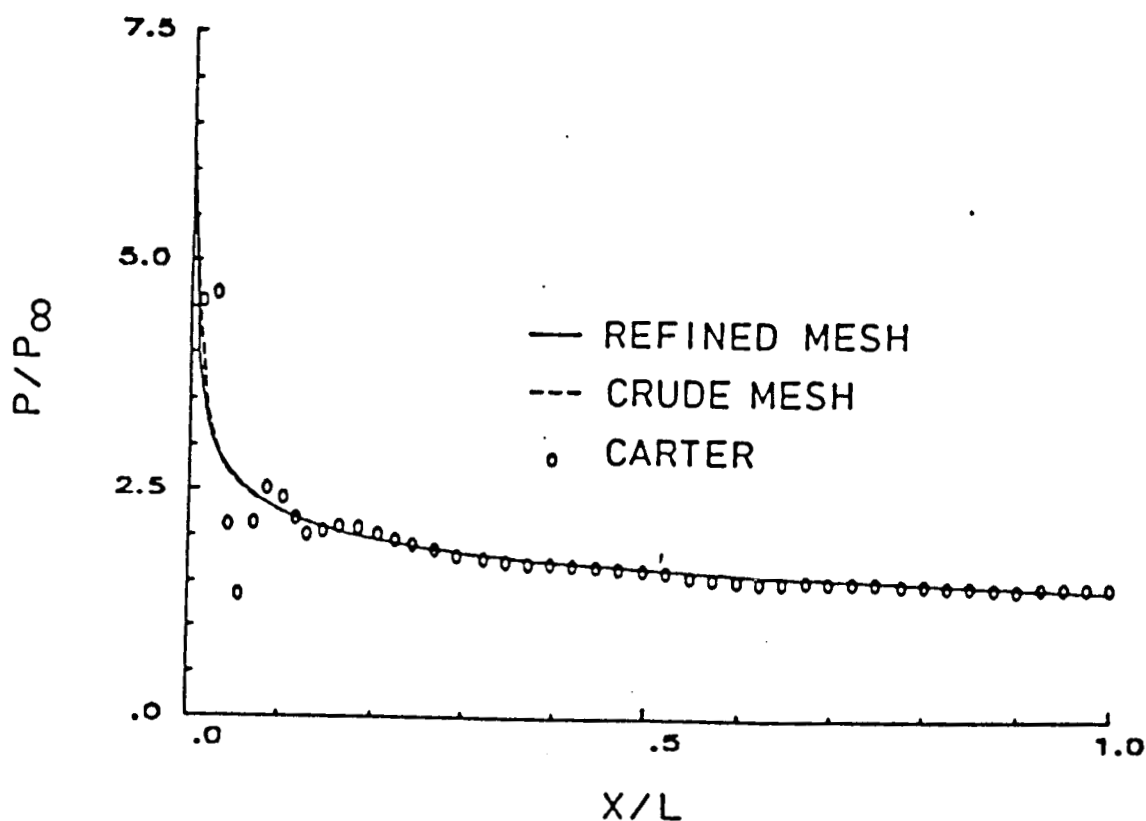


FIGURE 10

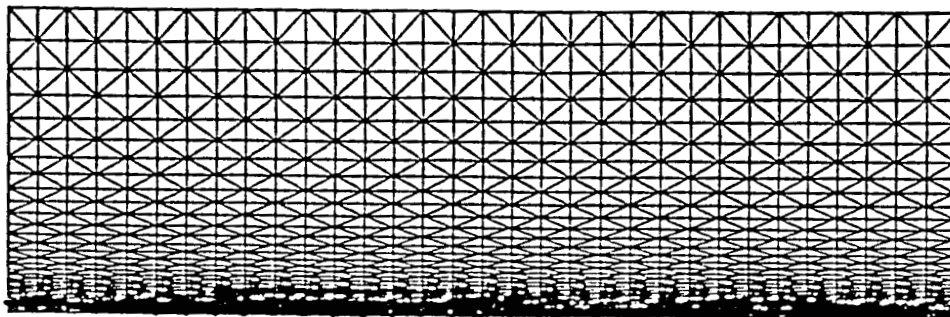
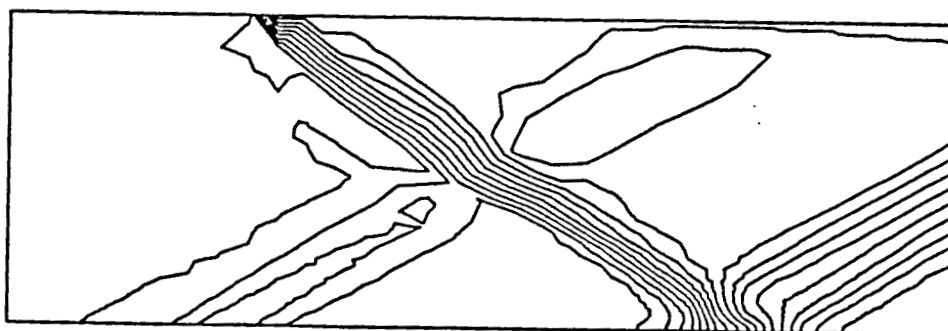


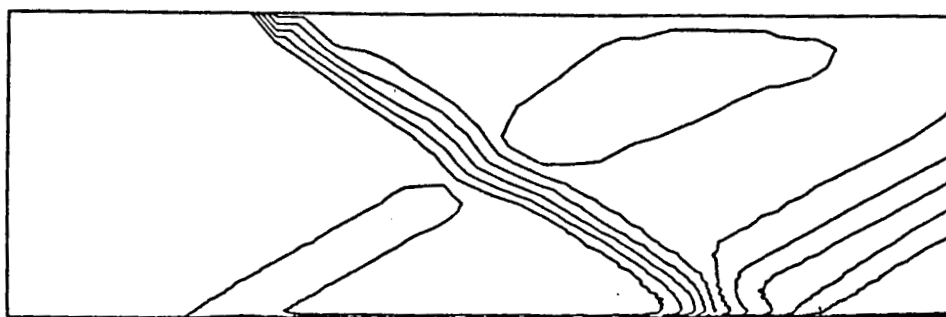
FIGURE 11

ORIGINAL PAGE IS
OF POOR QUALITY



PRESSURE

FIGURE 12



MACH

FIGURE 13

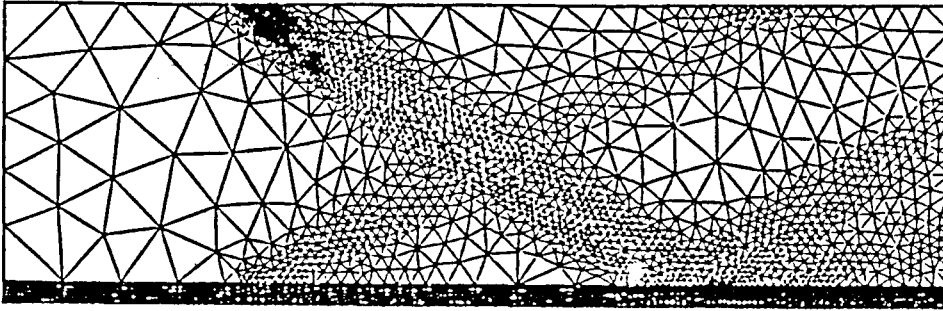
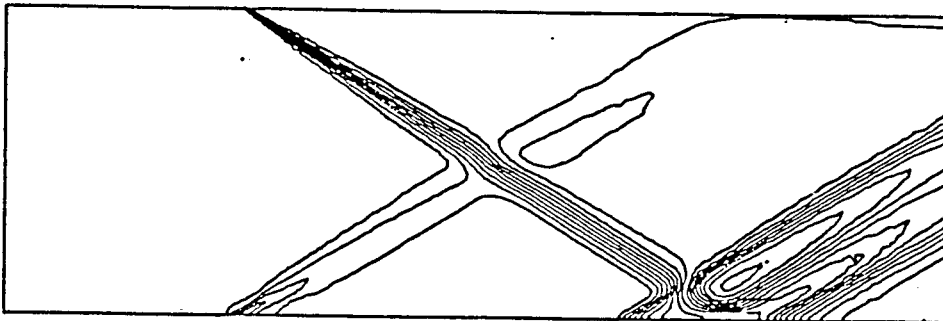


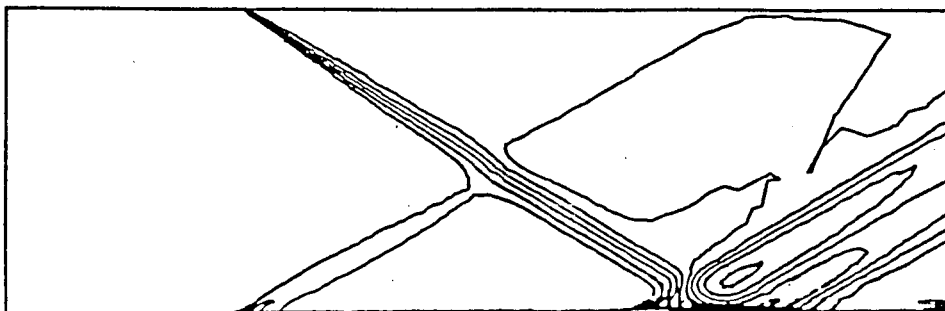
FIGURE 14

ORIGINAL PAGE IS
OF POOR QUALITY



PRESSURE

FIGURE 15



MACH

FIGURE 16

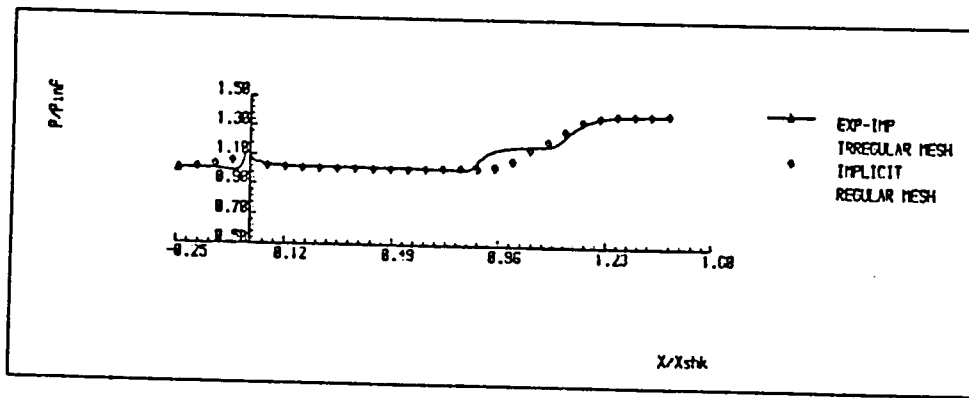


FIGURE 17 SURFACE PRESSURE

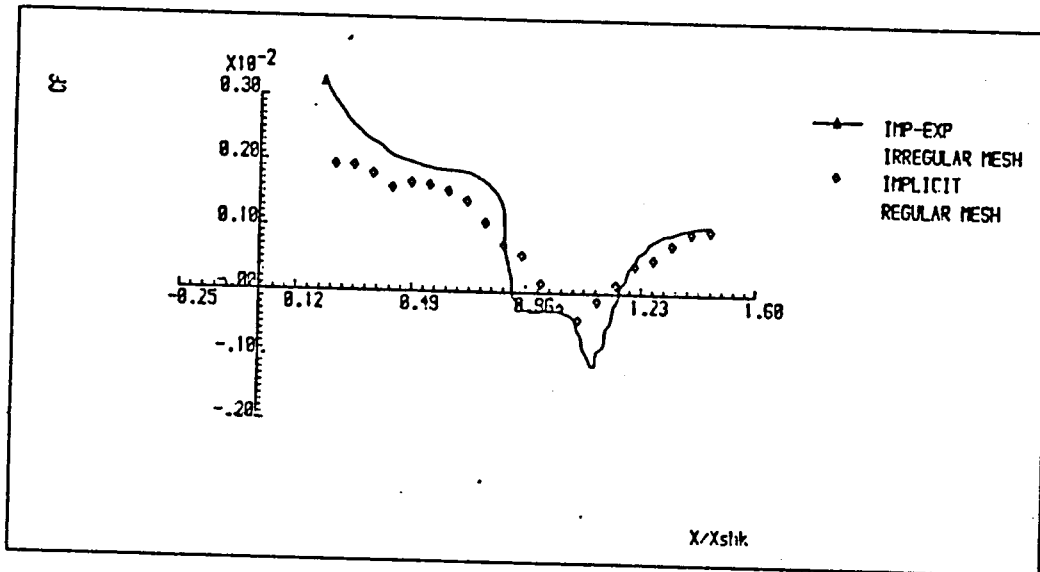


FIGURE 18 SKIN FRICTION

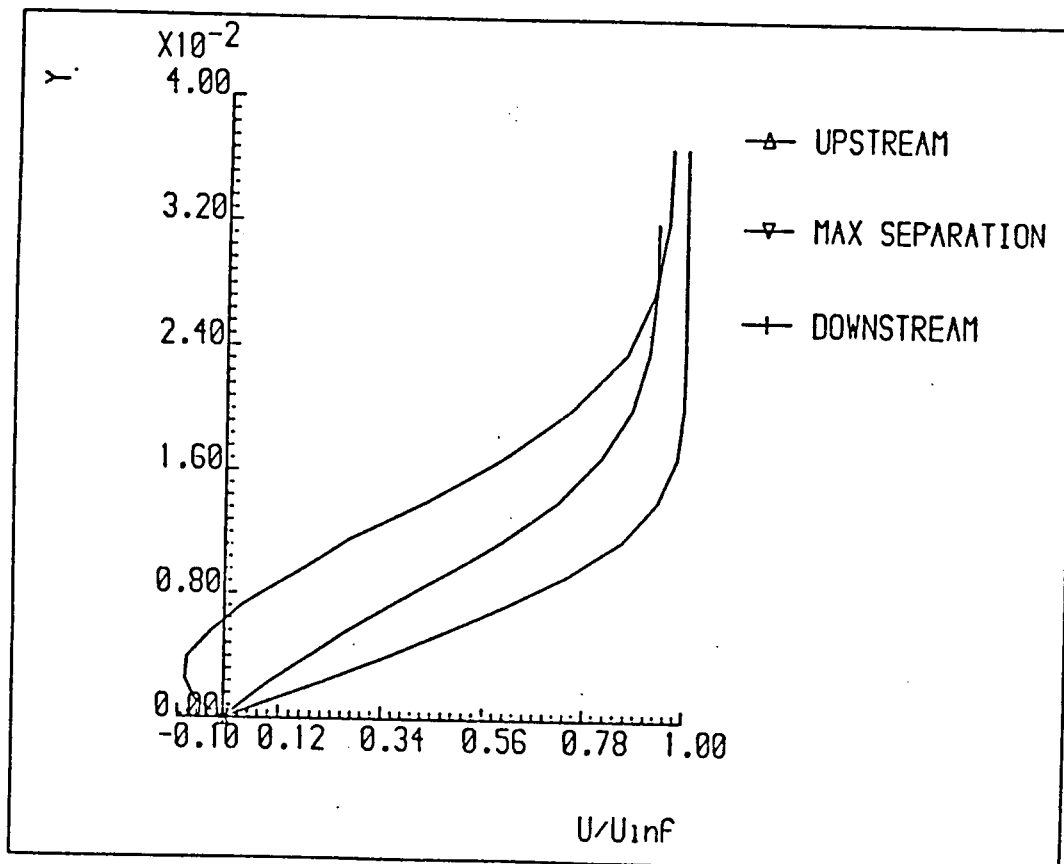


FIGURE 19 VELOCITY PROFILES

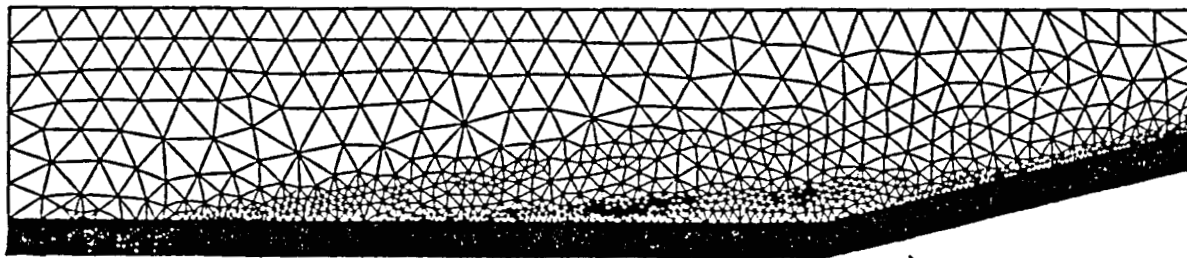


FIGURE 20

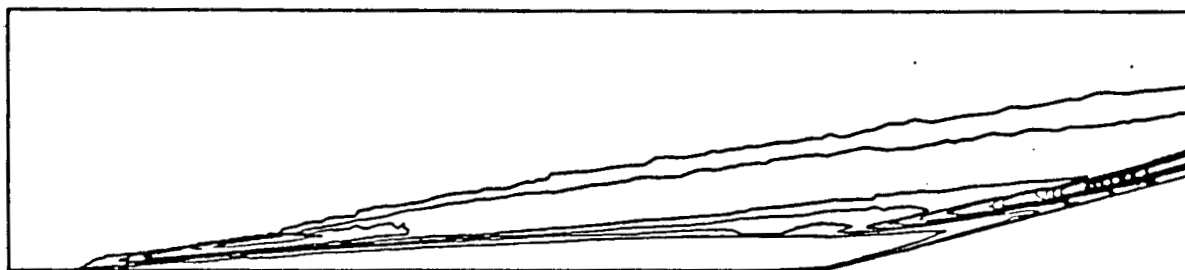


FIGURE 21

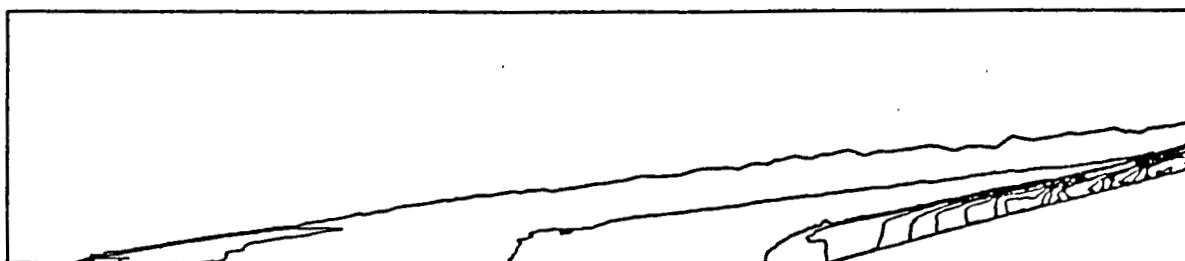


FIGURE 22

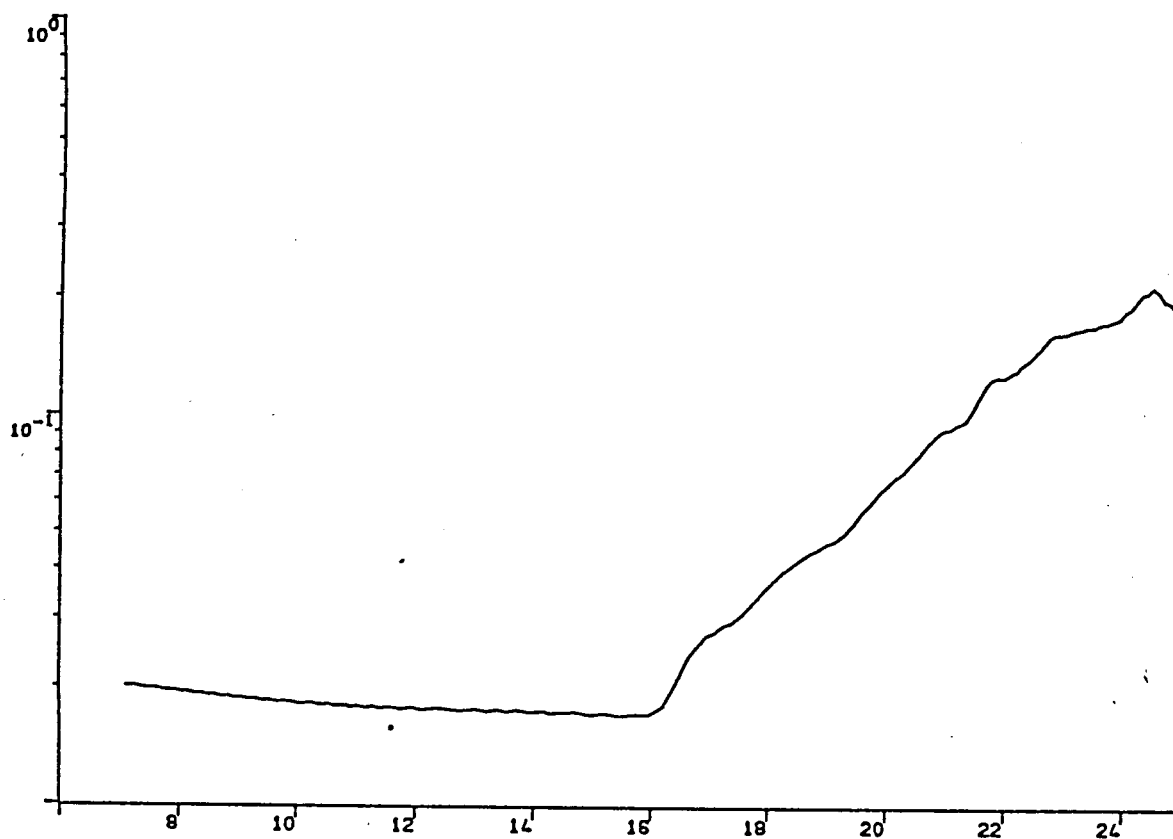


FIGURE 23

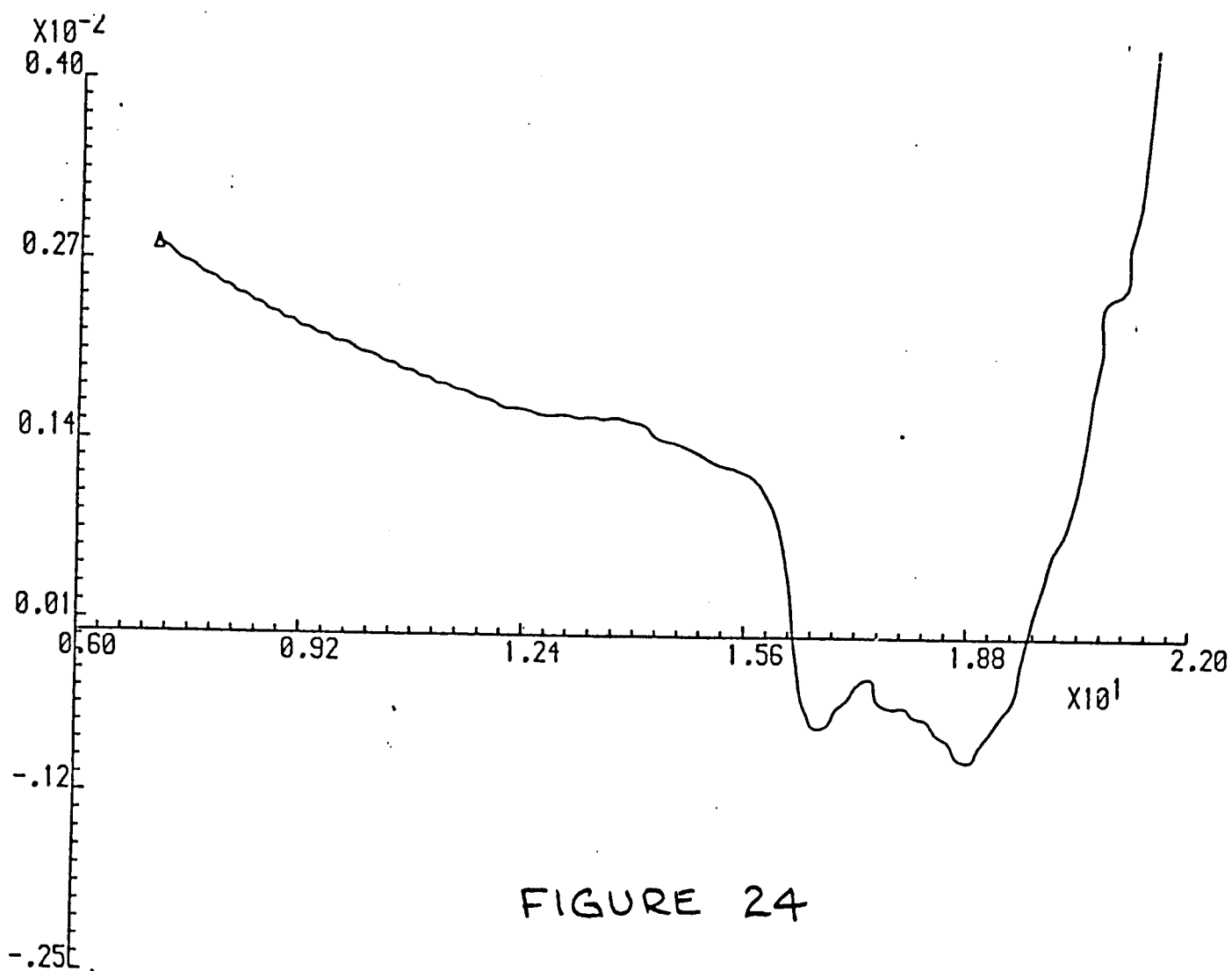
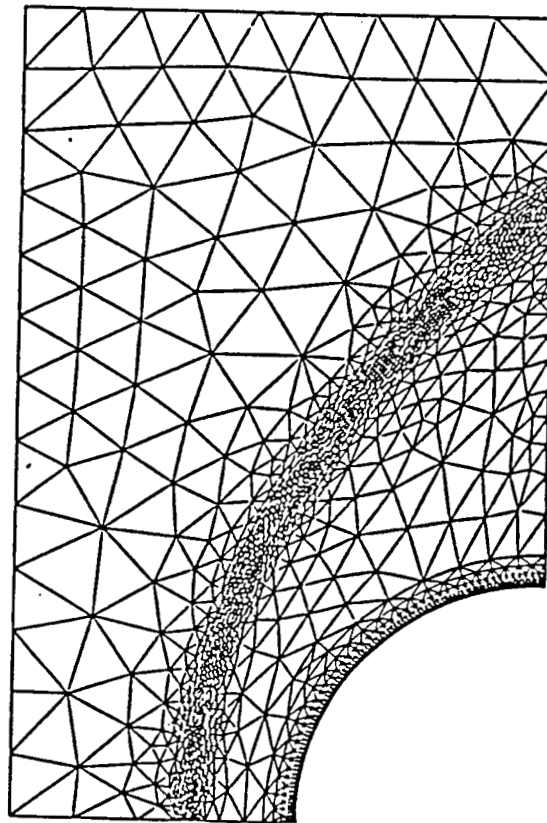


FIGURE 24



ORIGINAL PAGE IS
OF POOR QUALITY.

FIGURE 25



FIGURE 26

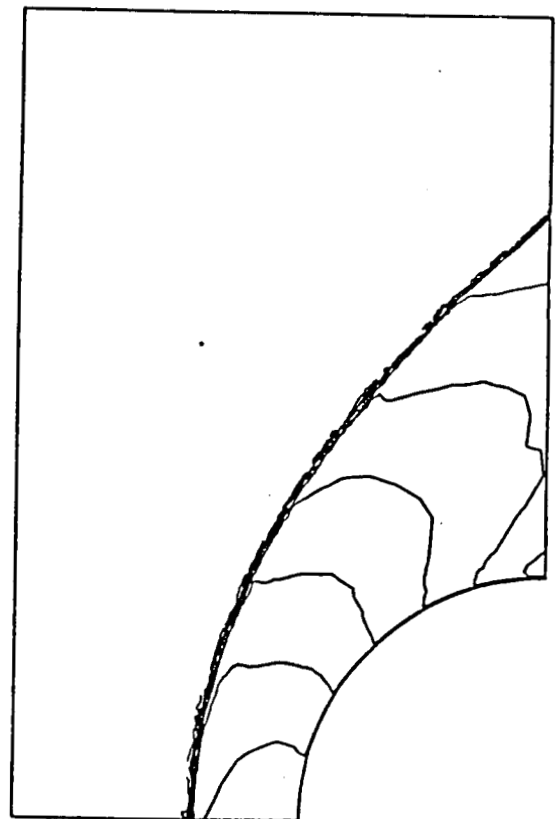


FIGURE 27

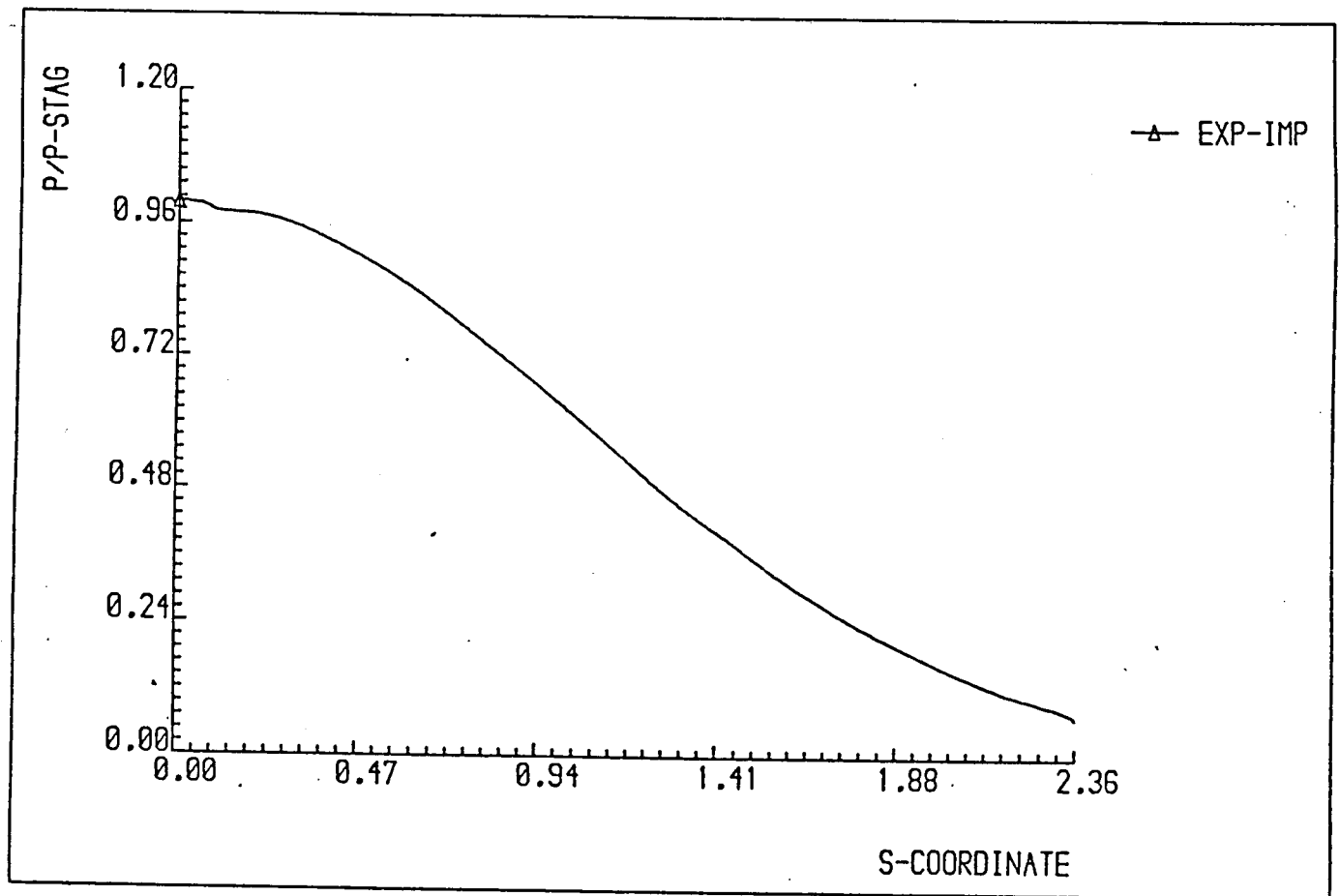


FIGURE 28 PRESSURE

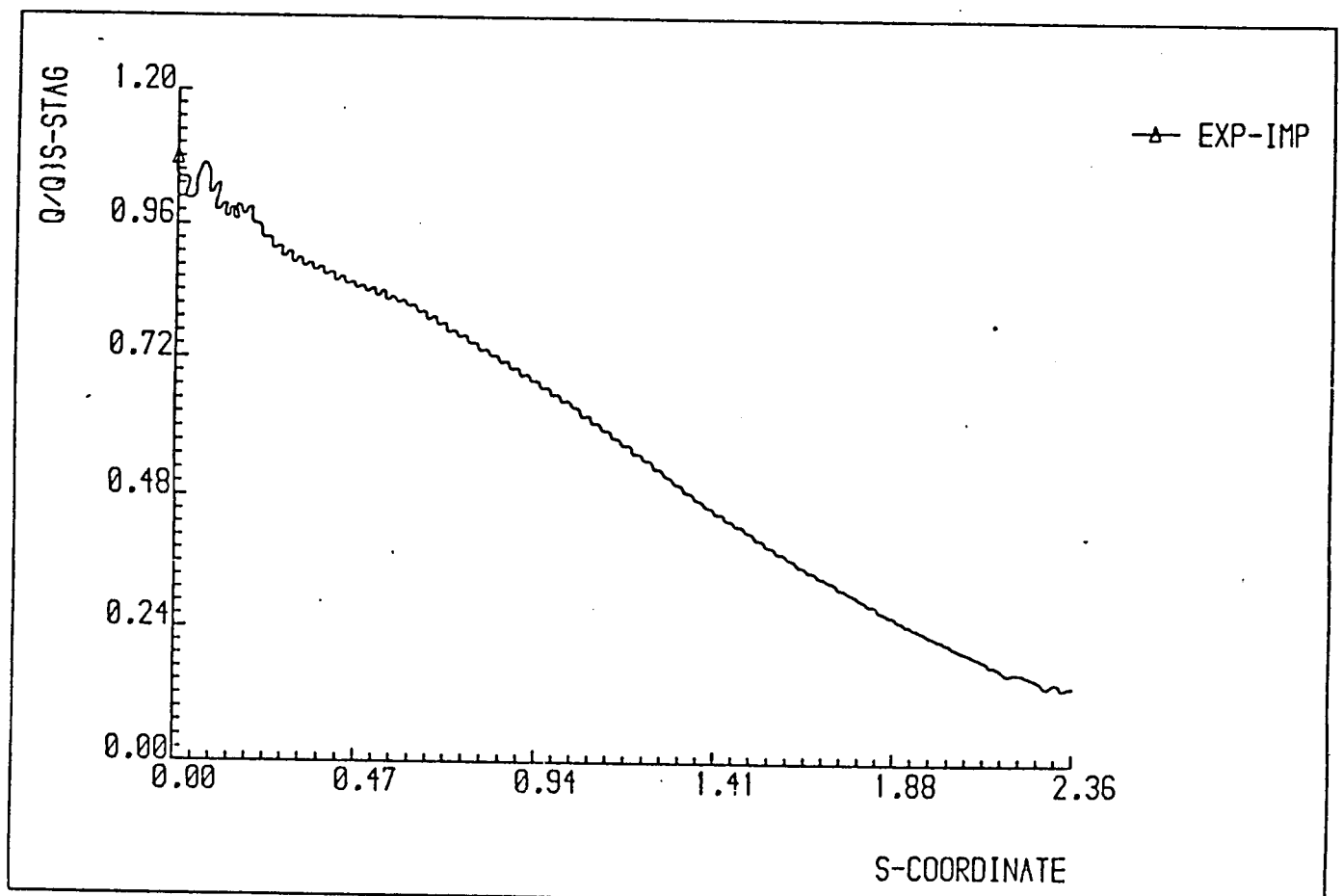


FIGURE 29 HEATING RATE